Anthropogenic forcing of the Northern Annular Mode in CCMVal-2 models

O. Morgenstern,[1] H. Akiyoshi,[2] S. Bekki,[3] P. Braesicke,[4] N. Butchart,[5]
M. P. Chipperfield,[6] D. Cugnet,[3] M. Deushi,[7] S. S. Dhomse,[6] R. R. Garcia,[8]
A. Gettelman,[8] N. P. Gillett,[9] S. C. Hardiman,[5] J. Jumelet,[3] D. E. Kinnison,[8]
J.-F. Lamarque,[8] F. Lott,[3] M. Marchand,[3] M. Michou,[10] T. Nakamura,[2] D. Olivié,[10]
T. Peter,[11] D. Plummer,[9] J. A. Pyle,[4] E. Rozanov,[11,12] D. Saint-Martin,[10] J. F. Scinocca,[9]
K. Shibata,[7] M. Sigmond,[13] D. Smale,[1] H. Teyssèdre,[10] W. Tian,[6] A. Voldoire,[10]
and Y. Yamashita[2,14]

[1] We address the question of how ozone and long-lived greenhouse gas changes impact the Northern Annular Mode (NAM). Using reanalyses and results from the Chemistry-Climate Model Validation 2 (CCMVal-2) initiative, we calculate seasonal NAM indices from geopotential height for winter and spring. From these, we determine the strength of stratosphere-troposphere coupling in the model simulations and the reanalyses. For both seasons, we find a large spread in the ability of models to represent the vertical coherence of the NAM, although most models are within the 95% confidence interval. In winter, many models underestimate the vertical coherence derived from the reanalyses. Some models exhibit substantial differences in vertical coherence between simulations driven with modeled and observed ocean conditions. In spring, in the simulations using modeled ocean conditions, models with poorer horizontal or vertical resolution tend to underestimate the vertical coupling, and vice versa for models with better resolution. Accounting for model deficits in producing an appropriate troposphere-stratosphere coupling, we show significant correlations of the NAM in winter with three indices representing the anthropogenic impact. Analysis of cross-correlations between these indices suggests that increasing CO_2 is the main reason for these correlations in this season. In the CCMVal-2 simulations, CO_2 increases are associated with a weakening of the NAM in winter. For spring, we show that the dominant effect is chemical ozone depletion leading to a transient strengthening of the NAM, with CO_2 changes playing an insignificant role.

Citation: Morgenstern, O., et al. (2010), Anthropogenic forcing of the Northern Annular Mode in CCMVal-2 models, *J. Geophys. Res.*, *115*, D00M03, doi:10.1029/2009JD013347.

1. Introduction

[2] Climate over the Northern Hemisphere has changed considerably during recent decades [*Intergovernmental Panel on Climate Change* (*IPCC*), 2007, Figure 3-10].

While summer and fall exhibit relatively small zonal variations and a relatively small overall warming of northern high latitudes, winter and spring are characterized by large differences in warming between the Eurasian and North American continents. During northern winter warming is

---

[1]National Institute of Water and Atmospheric Research, Lauder, New Zealand.
[2]National Institute of Environmental Studies, Tsukuba, Japan.
[3]LATMOS-IPSL, UVSQ, UPMC, CNRS/INSU, France.
[4]NCAS Climate Chemistry, Centre for Atmospheric Science, Chemistry Department, Cambridge University, Cambridge, UK.
[5]Hadley Centre, Met Office, Exeter, UK.
[6]School of Earth and Environment, University of Leeds, Leeds, UK.
[7]Meteorological Research Institute, Japan Meteorological Agency, Tsukuba, Japan.

[8]National Center for Atmospheric Research, Boulder, Colorado, USA.
[9]Canadian Centre for Climate Modeling and Analysis, Environment Canada, Victoria, British Columbia, Canada.
[10]GAME/CNRM, Météo-France, CNRS, Toulouse, France.
[11]Physical-Meteorological Observatory and World Radiation Center, Davos, Switzerland.
[12]Institute for Atmospheric and Climate Science, ETH Zürich, Zurich, Switzerland.
[13]Department of Physics, University of Toronto, Toronto, Ontario, Canada.
[14]Center for Climate System Research, University of Tokyo, Tokyo, Japan.

more pronounced in the North American Arctic than in Siberia, while in spring the opposite is found.

[3] Assessments of the causes of these trend patterns rely on atmosphere-ocean general circulation model (AOGCM) simulations, e.g., those discussed in the work of *IPCC* [2007]. In AOGCMs, climate change patterns can resemble the temperature signature of the Northern Annular Mode (NAM) [*Fyfe et al.*, 1999; *Shindell et al.*, 1999; *Baldwin*, 2001; *Shindell et al.*, 2001]; however, *Gillett* [2005] points out that deficits remain in modeling the pressure difference between high and low latitudes of the Northern Hemisphere, an important aspect of the NAM. This suggests widespread problems with the representation of this mode in AOGCMs and indicates that a better understanding of the mode and improved representations in models may be needed.

[4] Since around 1970, the NAM has shown an increase in variability and a pronounced strengthening trend until around 1990, followed by some more recent weakening [*Ostermeier and Wallace*, 2003; *IPCC*, 2007]. *Feldstein* [2002] finds that these variations cannot be explained by atmospheric internal variability alone (as established by the behavior of the NAM during the first 60 years of the 20th century); this implies either coupling with the hydrosphere/cryosphere or external forcing. The hypothesis that the anomalous variability is caused internally by atmosphere-ocean coupling is inconsistent with *Gillett* [2005]. *Overland and Wang* [2005] suggest however that there is decadal-scale intrinsic variability in the system which may mask any externally forced signal. The question remains whether the failure of the present generation of AOGCMs to capture the recent variations of the NAM [*Moritz et al.*, 2002; *Osborn*, 2004; *Gillett*, 2005] is a consequence of deficits in the model formulations affecting many AOGCMs, or whether the variations of the past 40 years are a rare unforced event which AOGCMs cannot be expected to reproduce. *Overland and Wang* [2005] also find that the decadal-scale variability of the NAM implies that climate trends in the Arctic, such as the surface warming reported in the work of *IPCC* [2007], depend strongly on the period considered. The World Meteorological Organization [*WMO*, 2007] states that the recent wintertime trends of the NAM are not explained by stratospheric ozone depletion. However, ozone depletion likely influences the NAM in spring, although the influence is thought to be weaker than that of increasing long-lived greenhouse gases (GHGs) [*Graf et al.*, 1998; *Volodin and Galin*, 1999; *Shindell et al.*, 2001]. *Kindem and Christiansen* [2001] find a strengthening of the NAM in March in response to ozone depletion. *Gillett et al.* [2003], while not mentioning the NAM, establish that GHGs and sulfate aerosol influence sea level pressure (SLP); however, models that only incorporate those two anthropogenic factors, underestimate the magnitude of the trends in SLP. The findings by *Gillett et al.* [2003] leave room for processes other than GHGs and sulfate aerosol to also play a role.

[5] A couple of studies have assessed the role of the stratosphere in shaping the NAM. *Shindell et al.* [1999] find a sensitivity of the NAM to the resolution of their model in the stratosphere, while *Scaife et al.* [2005] and *Douville* [2009] demonstrate that when their AOGCMs are constrained by the observed stratospheric circulation, the simulation of the NAM, as diagnosed from surface fields, does

exhibit realistic decadal-scale variability. *Sigmond et al.* [2008] find substantial differences in the NAM responses to increasing greenhouse gases between a model with and without a well resolved stratosphere. However, in their model, this difference is not caused by differences in model lid height but related to differences in model physics affecting lower stratospheric winds [*Sigmond and Scinocca*, 2010]. Their results thus indicate that the credibility of the NAM response to increasing greenhouse gases highly depends on how well a model simulates the lower stratospheric wind. These findings suggest an important role for stratospheric processes in driving the NAM, and provide a possible explanation why AOGCMs, mostly characterized by poor vertical resolution in the stratosphere and the absence of some stratospheric processes (e.g., ozone chemistry), do not produce a realistic simulation of the NAM.

[6] On the whole, we suggest that winter-spring variability of the NAM remains, at best, partly explained. Decadal-scale variability, occuring not just in the late 20th century but also in records spanning the last few centuries [*Cook et al.*, 2002; *Jones and Moberg*, 2003], complicates the picture. The important role of the stratosphere noted above suggests that stratospheric climate chemistry models (CCMs), with their improved resolution of the stratosphere and inclusion of stratospheric processes such as ozone chemistry, may be suitable tools to assess the ozone-climate interactions that possibly play a role in driving the NAM. CCM simulations spanning at least a century would be particularly helpful. Through the Chemistry Climate Model Validation (CCMVal) activity, such simulations have now become available.

[7] On the other hand, in almost all present-generation CCMs the ocean surface conditions are prescribed. *Hartmann et al.* [2000] suggest that feedbacks involving Arctic sea ice may be important factors in the future course of the NAM. *Hurrell et al.* [2004] find that coupling with the tropical ocean plays an important role in the observed variations of the NAM. Different CCMs driven with identical ocean boundary conditions, and indeed differences between ensemble members of the same model, can provide further insight into the role of oceanic forcing in CCMs. Prescribing ocean conditions means that near-surface climate must be regarded as partially externally imposed. *Scaife et al.* [2005], *Douville* [2009], and *Sigmond and Scinocca* [2010] suggest that CCMs including a more comprehensive representation of stratospheric processes may be in a better position to adequately represent the NAM than typical AOGCMs. For the Southern Hemisphere, *Son et al.* [2008] indicate a considerable impact of ozone depletion and recovery on the tropospheric polar jet [*Son et al.*, 2009], and substantial differences in the climate response between stratospheric CCMs and AOGCMs lacking an adequate representation of the stratosphere. By analogy to their Southern Hemisphere studies, a study of Northern Hemispheric lower-tropospheric climate change in CCM models may reveal interesting differences versus the equivalent results from AOGCMs, particularly in the northern middle and high latitudes where there is considerably more land than open ocean (where SSTs are imposed in CCMs). This is the topic of the present paper. We will assess the relationship between the NAM and anthropogenic

Table 1. Models Used Here, With Reference, Number of REF-B2/REF-B1 Simulations Used Here, Horizontal Resolution, Number of Levels, and Name of Parent Model Used for the Ocean Forcing in REF-B2[a]

CCM	Reference	Runs	Horizontal Resolution, Levels	SST/Sea Ice
CAM3.5	*Lamarque et al.* [2008]	1/1	$1.9° \times 2.50°$, L26	CCSM3
CCSRNIES	*Akiyoshi et al.* [2009]	1/1	T42L34	MIROC
CMAM	*Scinocca et al.* [2008]	3/3	T31L71	interactive
CNRM-ACM	*Teyssèdre et al.* [2007], *Déqué* [2007]	1/1	T42L60	CNRM-CM3
GEOSCCM	*Pawson et al.* [2008]	1[b]/1	$2.0° \times 2.50°$, L72	CCSM3
LMDZrepro	*Jourdain et al.* [2008]	1/3	$2.5° \times 3.75°$, L50	IPSL CM4
MRI	*Shibata and Deushi* [2008a, 2008b]	2/3	T42L68	MRI-GCM2.3.2
Niwa-SOCOL	*Schraner et al.* [2008]	1/1	T30L39	HadISST/HadGEM1
SOCOL	*Schraner et al.* [2008]	3/3	T30L39	ECHAM5-MPIOM
UMSLIMCAT	*Tian and Chipperfield* [2005]	1/1	$2.5° \times 3.75°$, L64	HadGEM1
UMUKCA-METO	*Morgenstern et al.* [2008, 2009]	1[c]/1	$2.5° \times 3.75°$, L60	HadGEM1
UMUKCA-UCAM	*Morgenstern et al.* [2008, 2009]	1/1	$2.5° \times 3.75°$, L60	HadGEM1
WACCM	*Garcia et al.* [2007]	3/4	$1.9° \times 2.50°$, L66	CCSM3

[a]Parent model simulations conform to the A1b scenario of *IPCC* [2007].
[b]GEOSCCM REF-B2 simulation only covers 2000–2099 and is therefore excluded from parts of the analysis performed here.
[c]UMUKCA-METO simulation covers 1960–2083.

forcings, using results from a multimodel climate chemistry modeling project outlined in section 2.

2. Data and Models

[8] We use data produced within the 2nd round of the CCMVal (CCMVal-2), a model intercomparison project which will inform the 2010 WMO ozone assessment [*Eyring et al.*, 2008]. Within this project, climate chemistry modelers were asked to simulate several scenarios. Here we mainly focus on the "REF-B2" experiments, which are seamless hindcasts and forecasts of ozone and other fields using best-known/best-estimate anthropogenic forcings and prescribed AOGCM ocean conditions or, in the case of one model, an interactive ocean (Table 1). SPARC Report No. 5 (SPARC Report on the Evaluation of Chemistry-Climate Models, WCRP-132, WMO/TD-No. 1526, edited by V. Eyring, T. G. Shepherd, and D. W. Waugh, 2010, available at http://www.atmosp.physics.utoronto.ca/SPARC) and *Morgenstern et al.* [2010] give details on the experiments and the participating models. To assess the impact of different ocean forcings, a few diagnostics are included using the "REF-B1" simulations. This set of simulations is restricted to the historical period (the years 1960–2004 are used here), and the models almost exclusively use observed HadISST [*Rayner et al.*, 2006] ocean conditions. The restriction to the historical period of the REF-B1 simulations means that climate effects due to ozone recovery cannot be derived from these simulations. Anthropogenic forcings of both sets of simulations are taken to follow the "modified" A1 (for ozone-depleting substances (ODSs)) [*WMO*, 2007] and A1b (for long-lived greenhouse gases (LLGHGs)) [*IPCC*, 2001] scenarios, respectively, meaning in the 21st century decreasing ODSs in accordance with the Montreal Protocol and its amendments, and a continuing increase of CO_2. (The "modified" A1 scenario assumes a faster phase-out of hydrogenated chlorofluorocarbons (HCFCs) than A1 but is otherwise unchanged; http://ozone.unep.org/Meeting_Documents/mop/19mop/Adjustments_on_HCFCs.pdf.) Variations in natural forcings (due to volcanic eruptions and the solar cycle) are excluded from the REF-B2 simulations; hence the focus is on anthropogenic forcings resulting from LLGHGs and ODSs. All models include comprehensive interactive stratospheric

chemistry. Table 1 lists the models whose data are used here, including references and a few selected model details. We use all available REF-B2 and REF-B1 simulations where sufficient data has been provided and tropospheric climate is not externally imposed.

[9] In addition to the CCMVal-2 data, we use seasonal-mean geopotential height (GPH) fields from the NCEP/NCAR [*Kalnay et al.*, 1996] and ERA-40 [*Uppala et al.*, 2005] reanalysis data sets, covering the periods 1960–2008 (NCEP/NCAR) and 1960–2001 (ERA-40), respectively. In comparisons with REF-B2 data, two volcanically affected years each after the eruptions of Agung (1963), El Chichón (1982), and Mt Pinatubo (1991), i.e., a total of 6 years, have been removed from the reanalysis data because volcanic forcing was excluded from the REF-B2 simulations.

3. Method

[10] We calculate the leading mode of variability (i.e., the NAM) and its interannual variations from modeled and reanalysis Northern Hemisphere seasonal-mean GPH fields, using an empirical orthogonal function (EOF) approach. The NAM is defined here as the leading EOF of GPH restricted to 1960–2008 and 1960–2004, respectively, for the REF-B2 and REF-B1 simulations. The method ensures that seasonal-mean variations in the strengths of the subtropical and polar jets are reflected in the NAM index while accounting for an expansion of the troposphere due to global warming. This means that a hypothetical uniform expansion of the Northern Hemisphere troposphere would not affect the NAM index. By contrast, deviations from a uniform expansion would be associated with a change in storminess and would affect the NAM indices produced here. The NAM is based on the restricted historical period to reduce any effect of changes to its shape associated with climate change in the REF-B2 simulations. All details of the analysis are in Appendix A. We thus derive, individually for every model/reanalysis, pressure level, and separately for the winter (DJF) and spring (MAM) seasons, a time series of seasonal mean GPH anomalies associated with the NAM. From these time series, we calculate vertical correlation functions, correlating the seasonal NAM index at 50 hPa to the seasonal NAM
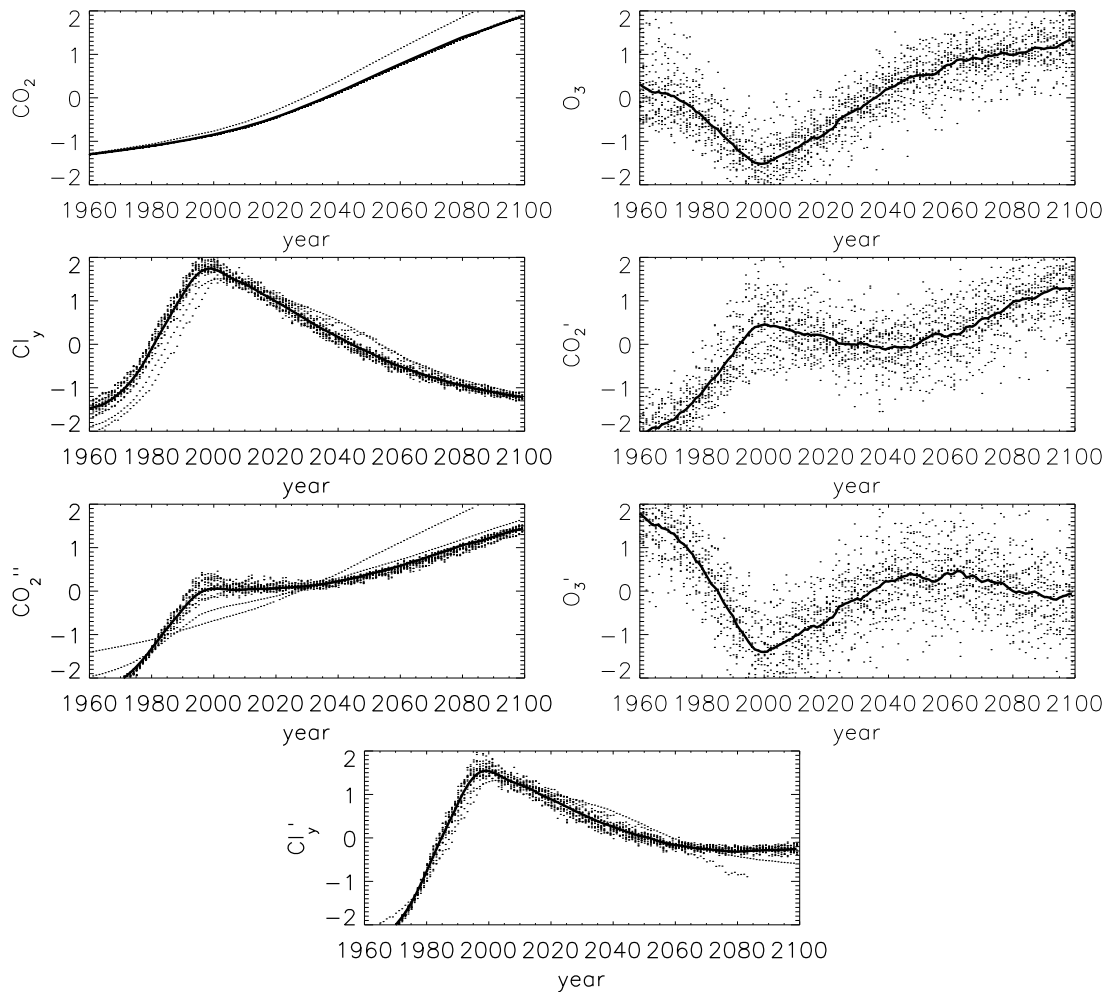
Figure 1. Forcing indices for the CCMVal-2 REF-B2 simulations, for the winter (DJF) season. For all variables the simulation mean has been subtracted and they have been divided by their standard deviation. Dots are individual model results. The thick black lines are the ensemble means, smoothed with a 7-year boxcar filter. CO_2: The CO_2 time series as defined in the A1b scenario. O_3: Hemispheric- and seasonal mean total ozone column. Cl_y: Hemispheric- and seasonal mean total inorganic chlorine at 50 hPa. CO'_2: Same as CO_2 but with the projection onto O_3 subtracted (equation (1)). CO''_2: Same as CO_2 but with the projection onto Cl_y subtracted. O'_3: Same as O_3 but with the projection onto CO_2 subtracted. Cl'_y: Same as Cl_y but with the projection onto CO_2 subtracted. Some outliers (e.g., evident in the CO_2 plot) are due to the UMUKCA-METO simulation covering a shorter period than the other simulations.

indices at other pressure levels. The analysis is similar to *Baldwin and Thompson* [2009]; it yields a measure of the degree of coupling (the "vertical coherence") within model simulations and reanalyses. The simulated vertical coherences are compared to those derived from the NCEP/ NCAR and ERA-40 reanalysis fields; to remain comparable, only the historical periods of the simulations (1960– 2008 for REF-B2, 1960–2004 for REF-B1) are used in the calculations of the vertical coherence, and in comparisons with REF-B2 simulations, volcanically affected periods are ignored in the reanalyses (section 2, Appendix A).

[11] In order to assess the anthropogenic influence, we define three different explanatory time series, organized as functions of season and year (Figure 1): (1) the prescribed uniform CO_2 abundance minus its simulation multiannual mean. This index is the same for all model simulations, and monotonically (albeit not linearly) increasing with time, in

accordance with the A1b scenario; (2) the hemispheric- and seasonal-mean column ozone minus its simulation-mean annual cycle; (3) the hemispheric- and seasonal-mean total inorganic chlorine (Cl_y) at 50 hPa, minus its simulation-mean annual cycle. The hemispheric indices are meant to broadly capture the anthropogenic influence while reducing the imprint of dynamically induced variability, evident for example in high-latitude ozone. By construction, the indices have a vanishing mean, and the ozone and Cl_y indices also have a vanishing mean annual cycle. We calculate correlation coefficients of the explanatory variables with the NAM at 850 hPa. This pressure is chosen as the lowest level which geopotential height is reported on where data is not overly affected by orography.

[12] We then perform two separate multilinear correlation analyses, using either the combination of the CO_2/O_3 series or of the CO_2/Cl_y series. The ozone and Cl_y time series are
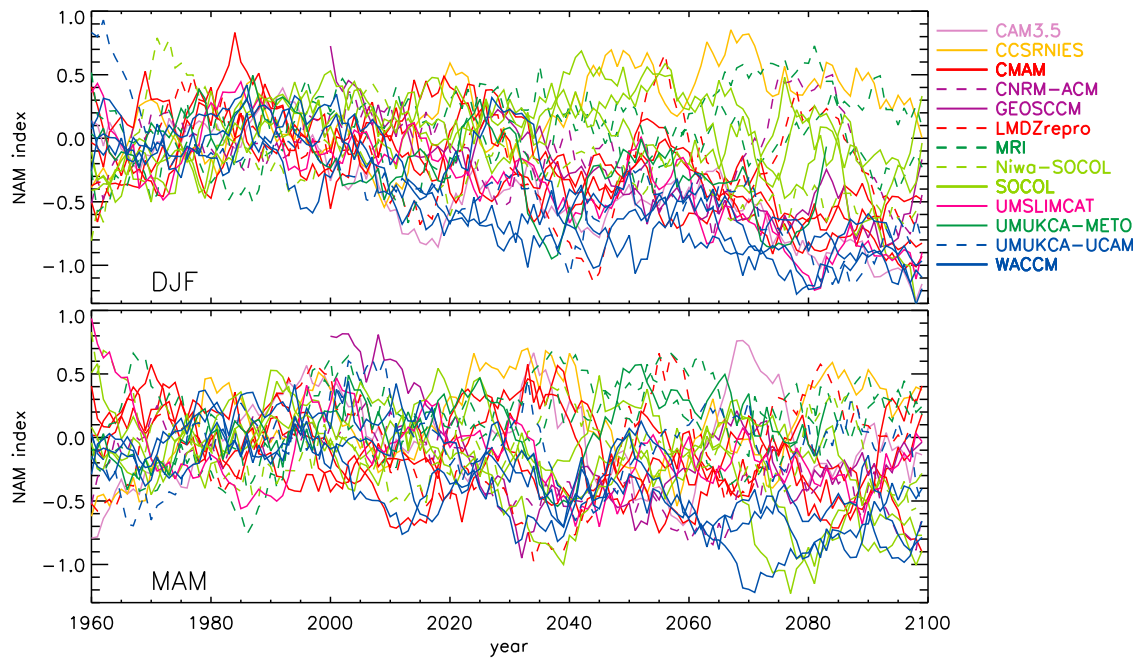
Figure 2. NAM indices, scaled to unit standard deviation, of the 20 REF-B2 simulations, for the (top) DJF and (bottom) MAM seasons. The indices have been smoothed with 11-year boxcar filters.

highly anticorrelated; mainly they differ in two respects: (1) Climate-change induced super-recovery affects the ozone but not the Cl_y time series, meaning that Cl_y is less correlated, in absolute terms, with CO_2 than ozone; and (2) dynamically induced interannual variability constitutes a much larger fraction of the total variability for ozone than for Cl_y. Nonetheless, both explanatory variables are retained here because ozone is more directly linked to dynamical variability than Cl_y, and Cl_y (and Br_y, whose influence would be statistically indistinguishable from Cl_y) are not the only agents causing ozone depletion. For example, recently contemporary N_2O emissions were identified as dominating the emissions of other ODSs in terms of their ozone-depletion potential [*Ravishankara et al.*, 2009]. N_2O is partially anthropogenic and undergoes substantial growth during the course of the REF-B2 simulations. However, N_2O is not considered here as an explanatory variable because its temporal evolution is too similar to that of CO_2.

[13] We perform the correlation analysis both with and without orthogonalizing the variables. The orthogonalization consists of subtracting the projections of the ozone/Cl_y indices onto CO_2 from those indices, i.e.,

$$x' = x - \frac{\langle x|y \rangle}{\langle y|y \rangle} y \qquad (1)$$

where x is the ozone or Cl_y index, x' is the orthogonalized index, y stands for the CO_2 index, and $\langle \cdot | \cdot \rangle$ is the vector product. Analogously, the projection of CO_2 onto ozone or Cl_y is subtracted off CO_2 using equation (1), where now x and x' stand for CO_2 (unmodified and with the projections removed) and y stands for O_3 and Cl_y, respectively. The resulting modified indices are displayed in Figure 1.

[14] Significance intervals for the correlation coefficients are determined at the 95% significance level (Appendix C). Correlating the NAM time series with the CO_2 index is not

exactly equivalent to performing a linear fit, due to CO_2 increasing nonlinearly with time (Figure 1). The terms "regression" and "correlation" are both used in this paper but are just different aspects of the same formalism (Appendix B).

[15] On a general note, interpreting correlations in non-stationary data requires care. Basically, when two variables exhibit trends (for example, the NAM and the CO_2 indices, see below), they will correlate even though there may not be any causal connection between the two. Inferring causal relationships thus requires further assumptions. Here we need to make the assumption that significant multidecadal trends only occur under the influence of changing external forcings. In this context, changing ocean conditions are not considered an independent external forcing but rather an aspect of global change induced by the changing composition of the atmosphere. Thus the analysis presented in section 4 could produce erroneous results if for example ocean surface conditions were subject to a drift which was not directly caused by the external forcings. While ruling out such problems for all models is beyond the scope of the paper, the fact that such drifts would have to occur coherently in different models using a range of different ocean forcings makes it unlikely that the results presented here are affected by this. We thus assume that any findings that occur coherently across the 13 models and 20 REF-B2 simulations analyzed here are caused by variations in the external forcings.

4. Results

4.1. NAM at 850 hPa

[16] We study the 850 hPa NAM first as this level is relatively close to the surface yet not overly affected by orography. Figure 2 shows the NAM indices of the 20 REF-B2 simulations for the winter and spring seasons.

Substantial intermodel differences are evident. Many models exhibit a negative trend in the latter part of the simulation which is more pronounced in winter than in spring. In spring, in some models the NAM index attains a maximum near the year 2000. Next, we assess the vertical structure of the NAM and the potential role of anthropogenic factors in driving the NAM.

4.2. Vertical Structure of the NAM

[17] Here we address how the tropospheric NAM is related to its stratospheric counterpart. This is motivated by the hypothesis that if changes in the ozone layer, or more generally stratospheric climate change, affect the tropospheric NAM, then a dynamical or radiative link between the tropospheric and stratospheric NAM would need to be established that conveys the stratospheric signal to the lower troposphere.

[18] Figure 3 shows the correlation of the NAM indices with the NAM index at 50 hPa separately for winter and spring, and separately for the REF-B2 and REF-B1 experiments. This diagnostic is similar to Figure 6 of *Baldwin and Thompson* [2009] except that here 100 hPa zonal-mean zonal wind is replaced with the NAM index at 50 hPa. The correlations obtained for the reanalyses (thick black lines) are numerically similar to those found by *Baldwin and Thompson* [2009]. In both seasons, the lower-tropospheric NAM correlates significantly (at the 95% level) with the 50 hPa NAM, and in winter the correlation is insignificantly stronger than in spring. (The significance is based on the spread of correlations inferred from a random permutation test described in Appendix C.) Both reanalyis datasets agree on this finding. Regarding the models, the following inferences can be made:

[19] 1. In winter (DJF), a majority of models underestimates the vertical coherence, both in the REF-B1 and REF-B2 simulations. However, most models remain within the 95% confidence interval associated with the vertical coherence inferred from the NCEP/NCAR reanalysis. In the REF-B2 simulation, CCSRNIES, WACCM, UMSLIMCAT, one SOCOL and one CMAM simulation are outside this interval. In REF-B1, CCSRNIES, UMSLIMCAT, and one CMAM simulation are outside the range.

[20] 2. In spring (MAM) the analyses are close to the center of the distribution. In the REF-B2 simulation, CMAM, CCSRNIES, and one SOCOL simulation produce too weak coupling. GEOSCCM produces the strongest coupling of the ensemble. For GEOSCCM, however, we consider a later period (Table 1), so it is not clear whether this is a model property. In REF-B1, CCSRNIES produces too weak coupling, and two WACCM simulations produce too strong coupling.

[21] 3. The diagnosis provides a consistency test for model ensembles. For example, in spring, the REF-B1 simulations of CMAM span a large range of vertical coherencies. This property sets the CMAM REF-B1 simulations apart from the CNRM-ACM, WACCM, MRI, and SOCOL REF-B1 ensembles which are statistically consistent in winter. It is unclear why vertical coherencies can span such a wide range, for identical external forcing. In the REF-B2 simulations, such inconsistencies do not occur.

[22] 4. Some interesting differences appear regarding the behavior of individual models in the REF-B2 and REF-B1 simulations. For example, CMAM is too incoherent in spring in the REF-B2 simulation but the three REF-B1 simulations exhibit a correct vertical coherence. SOCOL is likely too incoherent in REF-B2 but in REF-B1 produces a roughly correct vertical coherence in both seasons. An important difference between these two simulations relates to the ocean surface conditions (section 2). In the case of CMAM, the considerably different behavior between the two experiments may relate to the use of an interactive ocean in REF-B2 but observed ocean conditions in REF-B1. In the other cases, likewise the differences may be due to the AOGCM ocean forcings exhibiting biases versus observations (section 2). This is discussed in some more detail in section 5.

4.3. Correlation of the NAM With Anthropogenic Factors

[23] Having established how well models reproduce the deep coupling characterizing the NAM, we assess the roles of ozone, Cl_y, and LLGHGs in influencing the near-surface (850 hPa) NAM. Again, if stratospheric developments are responsible for surface trends, vertical coherence provides a mechanism explaining how stratospheric trends can affect surface climate.

[24] Unlike for the vertical coherence, here we cannot restrict the analysis to the historical period. Only when both ozone decline and recovery are included in the period of consideration, do ozone/Cl_y and CO_2 become sufficiently independent variables for this analysis. (For this reason, the GEOSCCM REF-B2 simulation is not considered in this part.)

[25] Figure 4 displays the correlation of the NAM index with the ozone/Cl_y and CO_2 indices, without orthogonalization of the explanatory variables. Absolute correlation coefficients greater than 0.17 can be considered statistically significant (Appendix C). The anomalous decrease of the absolute correlation for most simulations in the tropopause region may be an expression of a contamination of the leading EOF with the Pacific-North Atlantic pattern in this region [*Quadrelli and Wallace*, 2004, Appendix A]. Both in winter and in spring, almost all REF-B2 simulations agree that ozone changes anticorrelate and Cl_y changes correlate with the NAM, although the models disagree on the magnitude of these, and for some models the correlations are insignificant at the 95% level. The same analysis shows that for CO_2 the majority of models also indicate that there is an anticorrelation (meaning that CO_2 increases would be associated with a weakening of the NAM).

[26] In an effort to calculate a best estimate of the influences of ozone and CO_2 with the NAM, we plot the correlations with the explanatory variables at 850 hPa as functions of vertical coherence of the models (Figure 5). In this analysis, model simulations with erroneous vertical coupling have been omitted, namely CCSRNIES, WACCM, UMSLIMCAT, one CMAM, and one SOCOL simulation in winter and CMAM, CCSRNIES, and one SOCOL simulation in spring (Figure 3, top, and section 4.2). We have chosen not to remove simulations from this analysis which form part of an ensemble and other ensemble members produce erroneous vertical coupling. This applies to CMAM and SOCOL simulations in winter and only SOCOL in spring. Such a removal would constitute an unfair discrim-
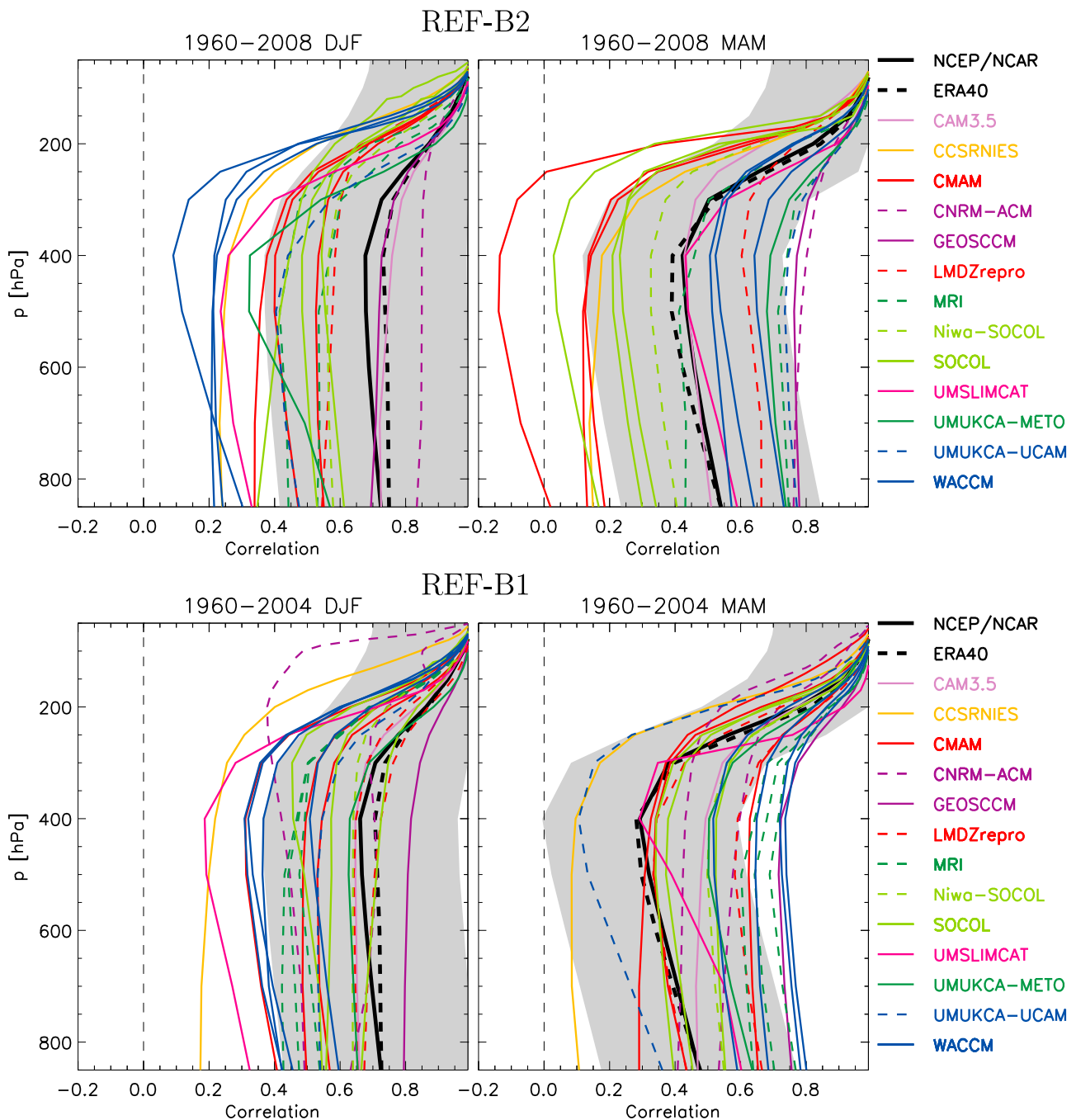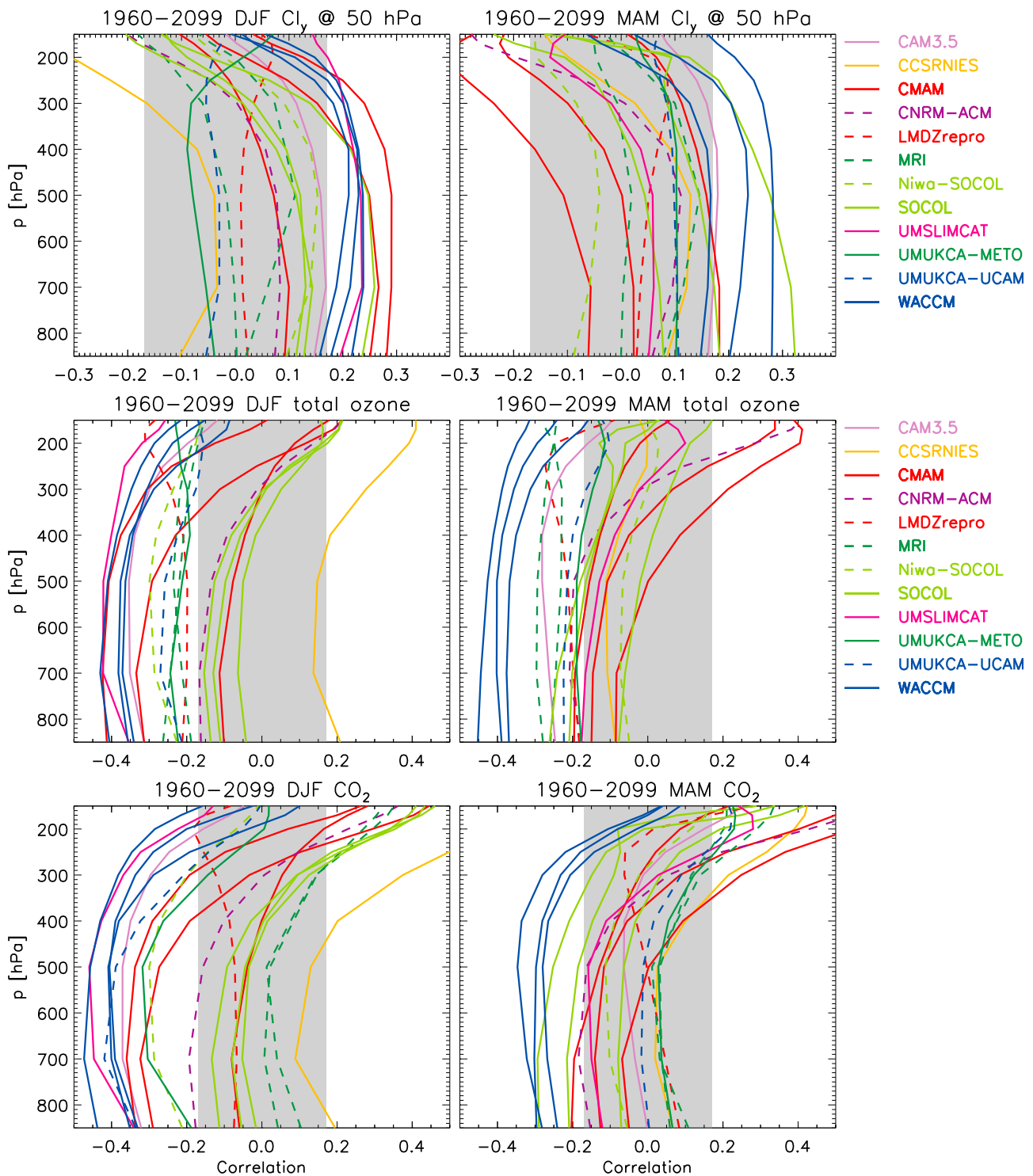
Figure 3. Correlation of the seasonal-mean NAM index, calculated as a function of pressure level from GPH fields, with the NAM index at 50 hPa, for the winter (DJF) and spring (MAM) seasons. (top) REF-B2 simulations and reanalyses for the years 1960–2008 (ERA-40: 1960–2001; GEOSCCM: 2000–2048). (bottom) REF-B1 and reanalyses for 1960–2004 (ERA-40: 1960–2001). For the models with multiple ensemble members, each member is represented separately.

ination of those models for which ensembles have been provided because other models which have contributed only one simulation cannot be dismissed on this ground. Also the fact that an acceptable vertical coherence is found in a simulation in itself increases credibility of any anthropogenic impact in this simulation, irrespectively of the behavior of other ensemble members.

[27] We then perform a linear regression through the remaining model results. Removing the outliers reduces the range of vertical coherence spanned by the models. The analysis provides a quantitative estimate of the correlation of the anthropogenic factors considered here with the NAM in the real atmosphere or in a hypothetical model with the same vertical coherence as in the NCEP/NCAR and ERA-40 reanalyses. In all situations depicted in Figure 5, except in spring for CO_2, a significant correlation is established. The error calculation used here is explained in detail in Appendix D. Removing the outliers also has the effect that

Figure 4. (top) Correlation of the seasonal mean NAM index, calculated as a function of pressure level from GPH fields, with the Cl_y index for the winter (DJF) and spring (MAM) seasons, for the full length of the REF-B2 simulations. Dashed lines represent CNRM-ACM, MRI, and UMUKCA-UCAM. (middle) Same, but for the ozone index. (bottom) Same, but for the CO_2 index. Correlations are significant at the 95% level if they are, in absolute terms, larger than approximately $2/\sqrt{n} = 0.17$, with $n = 140$ denoting the number of years in the NAM time series.
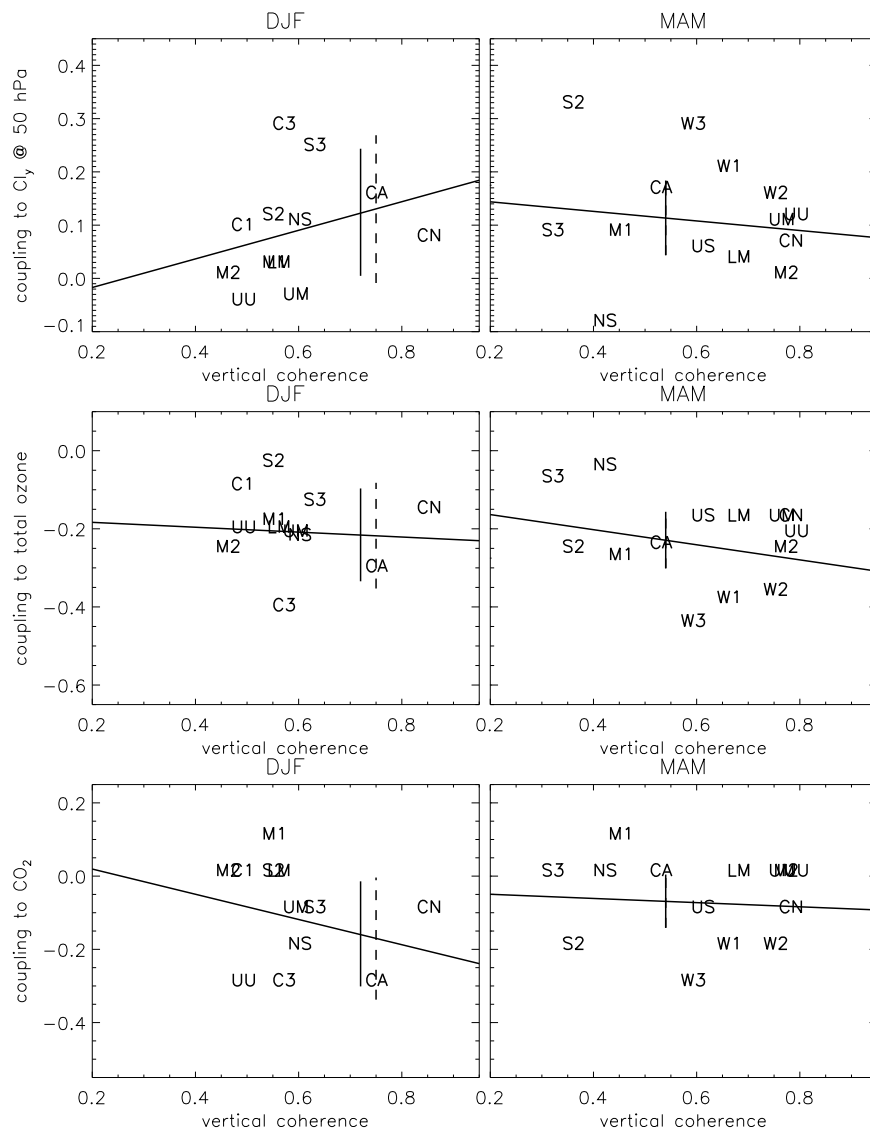
Figure 5. Scatterplots of vertical coherence versus the link with (top) hemispheric-mean 50 hPa Cl_y, (middle) the ozone index, and (bottom) CO_2 for the REF-B2 simulations. Simulations with erroneous vertical coherence have been omitted (see text). Abscissa: Correlation coefficient of the NAM index at 50 hPa with the NAM index at 850 hPa (Figure 3). Ordinate: Correlation coefficient of the three indices with the NAM at 850 hPa (Figure 4). Solid line: Linear least squares regression. Vertical lines: (solid) NCEP/NCAR, (dashed) ERA-40. The length of the lines corresponds to the 95% confidence interval. In spring, NCAP/NCAR and ERA-40 yield identical vertical coherences. CA = CAM3.5. Cx = CMAM. CN = CNRM-ACM. LM = LMDZrepro. Mx = MRI. NS = Niwa-SOCOL. Sx = SOCOL. US = UMSLIMCAT. UM = UMUKCA-METO. UU = UMUKCA-UCAM. Wx = WACCM. x = 1, 2, 3 stands for the ensemble members of the CMAM, MRI, SOCOL, and WACCM models.

generally there is no robust relationship between the vertical coherence and the impact of the anthropogenic factors. This suggests that for models that have an approximately realistic vertical coherence (i.e., a limited spread of vertical coherence), statistical variability and the influence of factors other than vertical coherence dominate the correlation with the anthropogenic variables.

[28] The results for the estimated impact of ozone/Cl_y and CO_2 changes in an atmosphere with the same vertical coherence as the NCEP/NCAR reanalyses are listed in Table 2. Using vertical coherence derived from ERA-40

data produces insignificantly different correlation coefficients. For comparison, if we ignored the systematic impact of vertical coherence errors (i.e., if we retained the outliers and calculated a straightforward multimodel mean of the correlation coefficients), the multimodel-mean ozone and CO_2 influences would be slightly underestimated in winter (Table 2, rows 4 and 9). In spring, however, accounting for these errors does not notably affect the results because the vertical coherence derived from the reanalyses occupies the center of the distribution spanned by the models.

Table 2. Best Estimate Correlation Coefficients of the O_3, Cl_y, and CO_2 Indices With the NAM Index[a]

	Season	
	DJF	MAM
1. CO_2 index	-0.16 ± 0.14	-0.07 ± 0.07
2. CO_2 index, projection onto O_3 subtracted	-0.03 ± 0.10	0.08 ± 0.07
3. CO_2 index, projection onto Cl_y subtracted	-0.12 ± 0.12	-0.03 ± 0.06
4. CO_2 index, vertical coherence uncorrected	-0.14 ± 0.14	-0.08 ± 0.06
5. CO_2 index, proj. onto smoothed O_3 subtracted	-0.09 ± 0.12	0.02 ± 0.05
6. O_3 index	-0.22 ± 0.11	-0.23 ± 0.07
7. O_3 index, projection onto CO_2 subtracted	-0.07 ± 0.13	-0.22 ± 0.08
8. O_3 index, smoothed	-0.19 ± 0.12	-0.12 ± 0.07
9. O_3 index, vertical coherence uncorrected	-0.21 ± 0.13	-0.20 ± 0.07
10. O_3 index, proj. onto CO_2 subtracted, smoothed	-0.00 ± 0.10	-0.06 ± 0.06
11. Cl_y index	0.12 ± 0.12	0.11 ± 0.07
12. Cl_y index, projection onto CO_2 subtracted	0.02 ± 0.12	0.07 ± 0.07

[a]See text and Figure 5. Row 1: Correlation coefficient of CO_2 with the NAM index. Row 2: Same as 1 but of the CO_2 index minus its projection onto ozone. Row 3: Same as 1 but of the CO_2 index minus its projection onto the Cl_y index. Row 4: Same as 1 but not accounting for deficits in vertical coherence (see text). Row 5: Same as 1 but of the CO_2 index minus its projection onto ozone smoothed with an 11-year boxcar filter. Row 6: Same as 1 but for the ozone index. Row 7: Same as 6 but for the ozone index minus its projection onto CO_2. Row 8: Same as 6 but with the ozone series smoothed with an 11-year boxcar filter. Row 9: Same as 6 but not accounting for deficits in vertical coherence. Row 10: Same as 6 but with the ozone series smoothed and with the projection onto CO_2 subtracted. Row 11: Same as 1 but for the Cl_y index. Row 12: Same as 11 but for the Cl_y index minus its projection onto CO_2.

[29] Figure 1 illustrates the considerable dynamically induced variability characterizing the ozone abundance. In an effort to make the ozone and chlorine correlations more comparable and to single out the anthropogenic component of ozone variability, we apply an 11-year boxcar filter to the ozone time series before calculating the correlation of the thus smoothed ozone with the NAM (Table 2, row 8). In spring (but not in winter), smoothing considerably reduces the correlation of ozone with the NAM, and the absolute correlation coefficient becomes almost the same as that of chlorine (row 11). This plausibly illustrates that in spring the correlation of ozone with the NAM is caused by both natural variability and by anthropogenic factors, with the anthropogenic influence being consistent with that of Cl_y. In winter, smoothing also reduces the correlation, but the correlation coefficient of the NAM with smoothed ozone is larger, in absolute terms, than that with Cl_y.

[30] We then repeat the analysis, however now accounting for the covariances of the ozone and Cl_y indices with CO_2 (rows 7 and 12). This means that in the regression analysis, the explanatory variables are now uncorrelated or "orthogonalized." In winter, the analysis reveals much reduced correlations of the NAM with Cl_y and ozone; the correlation with Cl_y is indistinguishable from 0, in this analysis. In addition applying an 11-year filter to the ozone time series reveals that the remaining correlation of ozone with the NAM in winter is due to seasonal-to-decadal coupling (rows 7 and 10). In spring, the correlations with ozone and

Cl_y remain significantly different from 0 (rows 7 and 12). Equivalently, the projections of CO_2 onto Cl_y or ozone are subtracted from CO_2 (rows 2 and 3). In spring, this turns a marginally significant anticorrelation into a similarly marginal correlation. In winter, however, subtracting the projection onto ozone makes the correlation of the remaining CO_2 time series with the NAM insignificant. Removing the projection onto Cl_y on the other hand has got an insignificant impact on the regression of CO_2 with the NAM. These results are discussed in more detail in section 5.

5. Discussion and Conclusions

[31] We have calculated best-estimate correlation coefficients between the NAM index and CO_2, the hemispheric mean total ozone column, and hemispheric mean Cl_y at 50 hPa. Different analyses have been performed without any modifications to the explanatory variables, with and without accounting for (mis)representations of the vertical coherence in models, with and without accounting for a coupling between the NAM and ozone on the seasonal to decadal timescale, and with and without accounting for covariances between CO_2 and ozone/Cl_y. A correlation analyis like ours using nonstationary data In winter, both ozone and CO_2 significantly anticorrelate with the NAM (Table 2, rows 1 and 6). We also find a smaller (in absolute terms) correlation with Cl_y (row 11). Subtraction of the projections onto CO_2 from the ozone/Cl_y indices shows that much of the correlations of the NAM with ozone/Cl_y is due a cross-correlation of these variables with CO_2 (rows 7 and 12). Effectively, removal of this covariance makes Cl_y uncorrelated and O_3 marginally correlated with the NAM. We show that the covariance of the thus modified ozone series is due to dynamically induced coupling on the seasonal-to-decadal timescale (rows 7 and 10).

[32] Conversely, removing the projections onto ozone from the CO_2 signal also makes the CO_2 signal uncorrelated (at the 95% confidence level) with the NAM (row 2). However, removing the projection onto Cl_y from CO_2 leaves the correlation largely intact (row 3). Rows 7 and 10 suggest that there are two reasons for the correlation of ozone with the NAM (row 6): (1) the pertinent trend in ozone (when this trend is removed, the correlation of ozone with the NAM is much reduced (row 7)) and (2) dynamically induced covariability. When a low-pass filter is applied to the ozone time series, in addition to removing the projection onto CO_2, smoothed ozone becomes uncorrelated with the NAM; this behavior is consistent with that of Cl_y (row 12). Together these results imply that ozone depletion does not significantly influence the NAM in winter.

[33] We note the negative sign of the correlation with CO_2 in winter, meaning that CO_2 increases, in these simulations, are associated a weakening of the NAM. This is in contrast to some earlier findings [e.g., *Shindell et al.*, 1999; *Eichelberger and Holton*, 2002; *Miller et al.*, 2006; *Stephenson et al.*, 2006]. This may be due to an acceleration of the Brewer-Dobson Circulation under climate change [*Butchart et al.*, 2006] leading to a warming and weakening of the polar vortex. Vertical coherence implies that this would have a weakening impact on the NAM. This effect may not be represented correctly in models lacking an adequately resolved stratosphere.

[34] In spring, the analysis finds a marginally significant influence of CO_2 but a substantial correlation of the NAM with ozone (Table 2, rows 1 and 6). The correlation with ozone is reduced but still significant if a low-pass filter is applied (rows 6 and 8), probably due to a dynamical linkage between the strength and longevity of the polar vortex, ozone, and the NAM. Applying the filter makes the results consistent between ozone and Cl_y (rows 8 and 11). We find that removing the projection onto CO_2 from the ozone and Cl_y time series leaves most of the correlation with the NAM intact (rows 7 and 12). We thus interpret that in spring the correlation of the NAM with ozone/Cl_y is likely substantially due to chemical ozone depletion.

[35] Generally, the role of ozone considered here underlines that stratospheric processes play an important role in shaping the near-surface NAM [*Scaife et al.*, 2005; *Douville*, 2009; *Sigmond and Scinocca*, 2010]. These results need to be compared to the established view that "Arctic ozone depletion has likely contributed to the weak positive trend in the NAM in the spring but cannot explain the observed winter trends" [*WMO*, 2007]. Our findings are broadly consistent with this statement. It does not account for ozone super-recovery because it refers only to past variations of the NAM. How much ozone depletion and climate change have contributed to the observed variations of the NAM cannot be directly inferred from our results because of the much longer time span, more progressive climate change, and ozone recovery characterizing the model data.

[36] In addition to *WMO* [2007], we find that increasing CO_2 is associated with a weakening of the NAM in winter; this weakening is probably linked to increasing CO_2 not just directly via the radiative forcing of CO_2 and associated dynamical changes but also indirectly via the impact of stratospheric climate change on the ozone layer. We do not find any impact of chemical ozone depletion on the NAM in winter.

[37] The present study is exclusively based on statistical evidence. An alternative approach would look for a mechanistic link between ozone changes and the NAM; such a study could be based on a suite of model simulations studying the NAM under the exclusion of manmade ozone depletion, or alternatively on a different suite of model simulations including manmade ozone depletion, but keeping long-lived greenhouse gases constant. Both of these groups of experiments are being prepared within CCMVal-2 (SCN-B2b and SCN-B2c in the work of *Eyring et al.* [2008]). Such a study would need a considerable number of simulations to analyze in order to reduce the impact of low-frequency variability. We will use the data when available to assess whether the anthropogenic influences in these simulations have the effects indicated by the statistical study performed here.

[38] The results indicate that horizontal and vertical resolution of the models may play a role in determining the strength of the link between ozone and the tropospheric NAM [see also *Braesicke et al.* 2008]. In Figure 3 (top) for spring those simulations showing less vertical coherence than indicated by the reanalyses are all characterized by relatively few levels in the stratosphere (Niwa-SOCOL, SOCOL, CCSRNIES), or a horizontal resolution of less than T42 (CMAM, Niwa-SOCOL, SOCOL; Table 1). This suggests, plausibly, that better resolution may help with improving vertical coherence [*Shindell et al.*, 1999]. How-

ever, conversely, those models with better resolution tend to display too much vertical coherence in spring, indicating that resolution is not the only factor causing erroneous vertical coupling. *Sigmond et al.* [2008] and *Sigmond and Scinocca* [2010] suggest that differences in the NAM response to increasing greenhouse gases between low- and high-top models may not be primarily due to vertical resolution in the stratosphere or the position of the model top. Instead, they find that the NAM response is sensitive to the lower stratospheric winds, which in their studies was induced by different settings in the orographic gravity wave drag. The models used here vary substantially regarding both resolution/model top and parameter settings; hence more research is needed to assess the role of orographic gravity wave drag in the results presented here. Also in winter, and in the REF-B1 simulations, this relationship of the vertical coherence with resolution does not hold. Interestingly, the model with the lowest lid and the fewest levels of the group considered here (CAM3.5) produces a vertical coherence which is closest to the reanalyses (Figure 5), illustrating this point.

[39] We note that our analysis leaves open the possibility that the dominant mode of variability may undergo changes of shape and not just amplitude. Such trends would be associated with progressive climate change and have likely not occurred during the period which reliable reanalysis data are available for. They can be assessed, for example, using separate EOF analyses for the beginnings and ends of the REF-B2 simulations. Our results may be partly the consequence of such shifts. An in-depth analysis of this problem is however beyond the scope of this paper.

[40] A remaining caveat in this study is that almost all models use prescribed ocean forcing. This imposes artificial constraints on the variability of surface climate and introduces a radiative imbalance into the models. A comparison of vertical coherence between the REF-B1 and REF-B2 simulations shows that individual models differ considerably between the two experiments, indicating that the ocean indeed plays an important role in conditioning vertical coherence. However, the general multimodel spread is about the same in REF-B1 and REF-B2, suggesting that the inter-model variability found in REF-B2 is not just the result of the imposition of different sea surface conditions. The lack of agreement on vertical coherence of the NAM of the models with the reanalyses in the REF-B1 simulations (Figure 3) helps explain the failure of models to capture recent variations in the strength of the near-surface NAM. The range spans models that do not exhibit any discernible response of the near-surface NAM to stratospheric changes to those that closely follow the stratospheric NAM and its changes. The representation of the NAM in climate models would benefit from directing efforts toward improving vertical coherence. Future chemistry-climate models will also likely comprise an interactive ocean (as does CMAM) [*Scinocca et al.*, 2008], allowing for a consistent simulation of the response of the climate system to anthropogenic forcings [*Hartmann et al.*, 2000]. *Kindem and Christiansen* [2001] argue that a strong response of the polar vortex to ozone depletion is needed for a significant signature of ozone depletion to be discernible in the troposphere. Our analysis suggests that erroneous vertical coherence of the NAM may also con-

tribute to models not producing an adequate tropospheric response to stratospheric changes.

[41] In summary, the CCMVal-2 REF-B2 simulations indicate that changing stratospheric ozone abundance significantly affects the seasonal-mean NAM in winter and spring over the REF-B2 period (1960–2099). In winter, its influence is mainly due to a coupling with stratospheric climate change, causing ozone super-recovery. In spring, the main reason is chemical ozone depletion.

Appendix A: Calculation of NAM Indices From Geopotential Height

[42] When calculating the NAM index from GPH fields, one encounters the problem that the GPH undergoes a substantial pertinent trend associated with an expansion of the troposphere, a consequence of global warming; this signal increases with height and can dominate variability. In the case of a hypothetical uniform expansion of the troposphere, associated geostrophic winds would not be affected by anything other than an upward shift, and one would like to adopt a definition of the NAM that would account for an upward shift of features but would otherwise not indicate a strengthening of the NAM. On the other hand, if there is a nonuniform expansion (as in reality), geostrophic winds are affected and this should be reflected as a trend in the NAM index. Accounting for these considerations, we employ the following procedure to derive the NAM from the data. Our definition is closely related to method 2 of *Baldwin and Thompson* [2009] but takes into account the slowly varying background state:

[43] 1. We start off with hemispheric monthly mean GPH fields $\Psi(\vec{r}, t)$, with $\vec{r} = (\lambda, \phi, p)$ denoting the spatial coordinates, from all REF-B1 and REF-B2 simulations considered here, and from the NCEP/NCAR and ERA-40 reanalyses.

[44] 2. In all subsequent steps, we remove data points from the analysis which would be placed below the Earth' surface (i.e., where the monthly mean surface pressure is less than the pressure characterizing the level, due to orography). This affects data points below 700 hPa.

[45] 3. In comparisons with REF-B2 data, we remove the periods March 1963 to February 1965, March 1982 to February 1984, and June 1991 to May 1993 from the reanalysis data as these are affected by the Agung, El Chichón, and Mt Pinatubo volcanic eruptions, respectively. This is because volcanic influences are ignored in the REF-B2 simulations.

[46] 4. For every simulation, month, and pressure level, we subtract the hemispheric mean GPH $\overline{\Psi}(p, t)$ and the mean annual cycle of the remainder, $\Psi_{\mathrm{mac}}(\vec{r}, \tau)$ calculated for the periods (REF-B2) 1960–2008 and (REF-B1) 1960–2004 (ERA-40: 1960–2002; GEOSCCM REF-B2: 2000–2048). (τ denotes the cyclical time variable characterizing the mean annual cycle.)

$$\Psi_1(\vec{r}, t) = \Psi(\vec{r}, t) - \overline{\Psi}(p, t) - \Psi_{\mathrm{mac}}(\vec{r}, \tau)$$

This means the hemispheric mean and the mean annual cycle of Ψ_1 are both identically 0.

[47] 5. Seasonal means Ψ_2 are calculated from Ψ_1. December of year $n - 1$ is counted as the first month of winter of year n. For winter 1960, we assume missing data.

[48] 6. We perform an empirical orthogonal function (EOF) analysis, based on the uniformly weighted covariance matrix, on Ψ_2, yielding, for every simulation, pressure level, and season, the mode and its associated time series (index). The domain of the analysis is the entire Northern Hemisphere. The index is rescaled to unit variance. We have verified that possible area weighting in the EOF analysis makes no tangible difference to the results. The sign of the mode is chosen such that the zonal-mean meridional gradient on average is negative, i.e., the mode is sloping downward toward the North Pole.

[49] The analysis is sensitive to dynamical trends in the GPH fields due to a lateral expansion of the upper troposphere (i.e., a poleward motion of the subtropical tropopause breaks) and an upward trend of the tropopause. Also *Quadrelli and Wallace* [2004] report that in upper-troposphere/lower-stratosphere region the Pacific-North Atlantic pattern interferes with the NAM as the leading mode. This explains the anomalous correlations with the explanatory variables (O_3, Cl_y, CO_2) in this pressure range in some simulations. Studying this region in more detail is beyond the scope of this paper.

Appendix B: Relationship Between Regression and Correlation Used Here

[50] Let n_i and m_i^j be time series, with n representing the NAM index and m^j the explanatory variables, all with vanishing mean and normalized so that $\|n\|^2 = = \Sigma_i n_i^2 = 1$ and $\|m^j\|^2 = = \Sigma_i (m_i^j)^2 = 1$. We expand n using a regression analysis:

$$n_i = \sum_j A^j m_i^j + \epsilon_i. \tag{B1}$$

Here, ϵ is the unexplained residual. By virtue of the regression analysis, ϵ_i does not correlate with the explanatory variables, and Pearson's correlation coefficient C^j evaluates to

$$C^j = \langle n | m^j \rangle = \sum_k A^k \langle m^k | m^j \rangle. \tag{B2}$$

Hence for orthogonalized, normalized explanatory variables we find $C^j = A^j$, i.e., the linear regression coefficients and Pearson's correlation coefficients are identical. If orthogonalization and normalization have not been applied, a linear transformation can be applied to derive one from the other. In this paper we use both concepts as appropriate.

[51] We note that the correlation coefficients for CO_2 and Cl_y with the NAM (Table 2) are straightforwardly converted into dimensional regression coefficients. For example, to calculate the regression coefficient of CO_2 with the NAM, the equation

$$a = c \frac{\sigma(\mathrm{NAM})}{\sigma(CO_2)} \tag{B3}$$

can be evaluated, where c is the correlation coefficient, a is the regression coefficient, and σ denotes the standard deviation. For CO_2, the standard deviation in the prescribed

A1b scenario for the period 1960–2099 is 207 ppmv, yielding a regression coefficient of the NAM with CO_2 in winter (Table 2, row 1) of $-7.7 \cdot 10^{-4} \sigma(NAM)/ppmv(CO_2)$. An analogous equation can be used for Cl_y. We approximate the standard deviation of inorganic chlorine at 50 hPa with that of prescribed total organic chlorine at the surface, which evaluates to 0.78 ppbv. This yields a regression coefficient of Cl_y with the NAM in winter (row 9) of $0.15\sigma(NAM)/ppbv(Cl_y)$. For ozone, an equivalent conversion would be model-specific due to the considerable spread in the response of modeled ozone to the anthropogenic forcings. The standard deviation of the NAM index depends on the definition of the NAM (Appendix A).

Appendix C: Derivation of Error Bars in Correlation Coefficients

[53] Using autocorrelation analysis we establish that the residual ϵ_i in equation (B1) does not have any substantial autocorrelation (i.e., neighboring data points can be considered uncorrelated). In this situation, an empirical approach known as a random permutation Monte Carlo simulation is valid whereby we construct ϵ' as a random permutation on the entries of ϵ. We then determine the correlation coefficients between ϵ' and the explanatory variables m_i^j. Iterating this procedure 10,000 times, we generate a cumulative probability density function (PDF) of the correlation coefficients. This PDF, for all explanatory variables, is centered on 0 (expressing that ϵ' is expected not to correlate with the explanatory variables). The 95% confidence interval is given by those correlation coefficients where the PDF evaluates to 2.5% and 97.5%, respectively. For a random time series with k entries, the 95% confidence interval is approximately given by $2k^{-1/2}$ or 0.17 for $k = 139$ or 140 (for REF-B2, in winter and spring, respectively). For the vertical coherence calculation, assuming no autocorrelation, k is 42 (in REF-B2 in winter), 43 (REF-B2, spring), 44 (REF-B1, winter), or 45 (REF-B1, spring), giving a 95% confidence error of 0.3. (Note again that for REF-B2, six volcanically perturbed years have been removed.)

Appendix D: Derivation of Error Bounds in the Calculation of the Best Estimate Correlation Coefficients

[54] In section 4.3, we derive the best estimate correlation coefficients by performing a linear regression, relating the individual correlation coefficients C_i to the vertical coherences, x_i. In this calculation, outliers as identified in section 4.2 have been removed. We define the linear regression by $C(x_i) = mx_i + b$ and the associated standard deviation μ as

$$\mu^2 = \frac{\sum [C_i - C(x_i)]^2}{M} \tag{D1}$$

where M is the number of remaining simulations after removal of the outliers. The combined standard deviation, also taking into account the standard deviation of the individual correlation coefficients, σ, is given by

$$\rho^2 = \mu^2 + \sigma^2. \tag{D2}$$

This assumes the individual unexplained remainders $C_i - C(x_i)$ are each associated with a Gaussian error distribution of width σ. Note that for a normally distributed variable, the standard deviation is approximately half the 95% confidence limit (determined in Appendix C).

[57] We then generate 10,000 realizations of sets of M pairs (x_i, χ_i) where the χ_i are normally distributed random numbers with a standard deviation of ρ. Evaluating the linear regressions through these realizations at the vertical coherences characterizing the NCEP/NCAR and ERA-40 reanalyses, we generate a cumulative PDF of the associated correlation coefficients. The positions where this PDF evaluates to 2.5% and 97.5% then determine the 95% confidence interval associated with the best estimate. Note that this confidence interval shrinks as the number of simulations M increases, due to the linear regression step involved.

References

Akiyoshi, H., L. B. Zhou, Y. Yamashita, K. Sakamoto, M. Yoshiki, T. Nagashima, M. Takahashi, J. Kurokawa, M. Takigawa, and T. Imamura (2009), A CCM simulation of the breakup of the Antarctic polar vortex in the years 1980–2004 under the CCMVal scenarios, *J. Geophys. Res.*, *114*, D03103, doi:10.1029/2007JD009103.

Baldwin, M. P. (2001), Annular modes in global daily surface pressure, *Geophys. Res. Lett.*, *28*, 4114–4118.

Baldwin, M. P., and D. W. J. Thompson (2009), A critical comparison of stratosphere–troposphere coupling indices, *Q. J. R. Meteorol. Soc.*, *135*, 1661–1672, doi:10.1002/qj.479.

Braesicke, P., et al. (2008), A model intercomparison analysing the link between column ozone and geopotential height anomalies in January, *Atmos. Chem. Phys.*, *8*, 2519–2535.

Butchart, N., et al. (2006), Simulations of anthropogenic change in the strength of the Brewer–Dobson circulation, *Clim. Dyn.*, *27*, 727–741, doi:10.1007/s00382-006-0162-4.

Cook, E. R., R. D. D'Arrigo, and M. E. Mann (2002), A well-verified, multiproxy reconstruction of the winter North Atlantic Oscillation index since A. D. 1400, *J. Clim.*, *15*, 1754–1764.

Déqué, M. (2007), Frequency of precipitation and temperature extremes over France in an anthropogenic scenario: Model results and statistical correction according to observed values, *Global Planet. Change*, *57*, 16–26.

Douville, H. (2009), Stratospheric polar vortex influence on Northern Hemisphere winter climate variability, *Geophys. Res. Lett.*, *36*, L18703, doi:10.1029/2009GL039334.

Eichelberger, S. J., and J. R. Holton (2002), A mechanistic model of the Northern Annular Mode, *J. Geophys. Res.*, *107*(D19), 4388, doi:10.1029/2001JD001092.

Eyring, V., M. P. Chipperfield, M. A. Giorgetta, D. E. Kinnison, E. Manzini, K. Matthes, P. A. Newman, S. Pawson, T. G. Shepherd, and D. W. Waugh (2008), Overview of the new CCMVal reference and sensitivity simulations in support of upcoming ozone and climate assessments and the planned SPARC CCMVal, *SPARC Newsl.*, *30*, 20–26.

Feldstein, S. B. (2002), The recent trend and variance increase of the Annular Mode, *J. Clim.*, *15*, 88–94.

Fyfe, J. C., G. J. Boer, and G. M. Flato (1999), The Arctic and Antarctic oscillations and their projected changes under global warming, *Geophys. Res. Lett.*, *26*, 1601–1604.

Garcia, R. R., D. R. Marsh, D. E. Kinnison, B. A. Boville, and F. Sassi (2007), Simulation of secular trends in the middle atmosphere, 1950–2003, *J. Geophys. Res.*, *112*, D09301, doi:10.1029/2006JD007485.

Gillett, N. P. (2005), Northern Hemisphere circulation, *Nature*, *437*, 496, doi:10.1038/437496a.

Gillett, N. P., F. W. Zwiers, A. J. Weaver, and P. A. Stott (2003), Detection of human influence on sea-level pressure, *Nature*, *422*, 292–294.

Graf, H. F., I. Kirchner, and J. Perlwitz (1998), Changing lower stratospheric circulation: The role of ozone and greenhouse gases, *J. Geophys. Res.*, *103*, 11,251–11,261.

Hartmann, D. L., J. M. Wallace, V. Limpasuvan, D. W. J. Thompson, and J. R. Holton (2000), Can ozone depletion and global warming interact to produce rapid climate change?, *Proc. Natl. Acad. Sci. U. S. A.*, *97*, 1412–1417.

Hurrell, J. W., M. P. Hoerling, A. S. Phillips, and T. Xu (2004), Twentieth century North Atlantic climate change. Part 1: Assessing determinism, *Clim. Dyn.*, *23*, 371–389.

Intergovernmental Panel on Climate Change (IPCC) (2001), *Climate Change 2001: Working Group I: The Scientific Basis*, Cambridge Univ. Press, New York.

IPCC (2007), *Climate Change 2007: The Physical Science Basis. Contribution of Working Group I to the Fourth Assessment Report of the Intergovernmental Panel on Climate Change*, edited by S. Solomon et al., 996 pp., Cambridge Univ. Press, New York.

Jones, P. D., and A. Moberg (2003), Hemispheric and large-scale surface air temperature variations, An extensive revision and update to 2001, *J. Clim.*, *16*, 206–223.

Jourdain, L., S. Bekki, F. Lott, and F. Lefèvre (2008), The coupled chemistry-climate model LMDz-REPROBUS: Description and evaluation of a transient simulation of the period 1980–1999, *Ann. Geophys.*, *26*(6), 1391–1413.

Kalnay, E., et al. (1996), The NCEP/NCAR 40-year reanalysis project, *Bull. Am. Meteorol. Soc.*, *77*, 437–470.

Kindem, I. T., and B. Christiansen (2001), Tropospheric response to stratospheric ozone loss, *Geophys. Res. Lett.*, *28*, 1547–1550.

Lamarque, J.-F., D. E. Kinnison, P. G. Hess, and F. M. Vitt (2008), Simulated lower stratospheric trends between 1970 and 2005: Identifying the role of climate and composition changes, *J. Geophys. Res.*, *113*, D12301, doi:10.1029/2007JD009277.

Miller, R. L., G. A. Schmidt, and D. T. Shindell (2006), Forced annular variations in the 20th century Intergovernmental Panel on Climate Change Fourth Assessment Report models, *J. Geophys. Res.*, *111*, D18101, doi:10.1029/2005JD006323.

Morgenstern, O., P. Braesicke, M. M. Hurwitz, F. M. O'Connor, A. C. Bushell, C. E. Johnson, and J. A. Pyle (2008), The World Avoided by the Montreal Protocol, *Geophys. Res. Lett.*, *35*, L16811, doi:10.1029/2008GL034590.

Morgenstern, O., P. Braesicke, F. M. O'Connor, A. C. Bushell, C. E. Johnson, S. M. Osprey, and J. A. Pyle (2009), Evaluation of the new UKCA climate-composition model – Part 1: The stratosphere, *Geosci. Model Dev.*, *2*, 43–57.

Morgenstern, O., et al. (2010), Review of the formulation of present-generation stratospheric chemistry-climate models and associated external forcings, *J. Geophys. Res.*, *115*, D00M02, doi:10.1029/2009JD013728.

Moritz, R. E., C. M. Bitz, and E. J. Steig (2002), Dynamics of recent climate change in the Arctic, *Science*, *297*, 1497–1502.

Osborn, T. J. (2004), Simulating the winter North Atlantic Oscillation: The roles of internal variability and greenhouse forcing, *Clim. Dyn.*, *22*, 605–623.

Ostermeier, G. M., and J. M. Wallace (2003), Trends in the North Atlantic Oscillation–Northern–Hemisphere annular mode during the twentieth century, *J. Clim.*, *16*, 336–341.

Overland, J. E., and M. Wang (2005), The Arctic climate paradox: The recent decrease of the Arctic Oscillation, *Geophys. Res. Lett.*, *32*, L06701, doi:10.1029/2004GL021752.

Pawson, S., R. S. Stolarski, A. R. Douglass, P. A. Newman, J. E. Nielsen, S. M. Frith, and M. L. Gupta (2008), Goddard Earth Observing System chemistry-climate model simulations of stratospheric ozone-temperature coupling between 1950 and 2005, *J. Geophys. Res.*, *113*, D12103, doi:10.1029/2007JD009511.

Quadrelli, R., and J. M. Wallace (2004), A simplified linear framework for interpreting patterns of Northern Hemisphere wintertime climate variability, *J. Clim.*, *17*, 3728–3744.

Ravishankara, A. R., J. S. Daniel, and R. W. Portmann (2009), Nitrous oxide (N_2O): The dominant ozone-depleting substance emitted in the 21st century, *Science*, *326*, 123–125, doi:10.1126/science.1176985.

Rayner, N. A., P. Brohan, D. E. Parker, C. K. Folland, J. J. Kennedy, M. Vanicek, T. Ansell, and S. F. B. Tett (2006), Improved analyses of changes and uncertainties in sea surface temperature measured in situ since the mid-nineteenth century: The HadISST2 data set, *J. Clim.*, *19*, 446–469.

Scaife, A. A., J. R. Knight, G. K. Vallis, and C. K. Folland (2005), A stratospheric influence on the winter NAO and North Atlantic surface climate, *Geophys. Res. Lett.*, *32*, L18715, doi:10.1029/2005GL023226.

Schraner, M., et al. (2008), Technical Note: Chemistry-climate model SOCOL: Version 2.0 with improved transport and chemistry/microphysics schemes, *Atmos. Chem. Phys.*, *8*, 5957–5974.

Scinocca, J. F., N. A. McFarlane, M. Lazare, J. Li, and D. Plummer (2008), Technical Note: The CCCma third generation AGCM and its extension into the middle atmosphere, *Atmos. Chem. Phys.*, *8*, 7055–7074.

Shibata, K., and M. Deushi (2008a), Long-term variations and trends in the simulation of the middle atmosphere 1980–2004 by the chemistry-climate model of the Meteorological Research Institute, *Ann. Geophys.*, *26*, 1299–1326.

Shibata, K., and M. Deushi (2008b), Simulation of the stratospheric circulation and ozone during the recent past (1980–2004) with the MRI chemistry-climate model, *Supercomputer Monogr. Rep. 13*, 154 pp., Natl. Inst. for Environ. Stud., Tsukuba, Japan.

Shindell, D. T., R. L. Miller, G. A. Schmidt, and L. Pandolfo (1999), Simulation of recent northern winter climate trends by greenhouse-gas forcing, *Nature*, *399*, 452–455.

Shindell, D. T., G. A. Schmidt, R. L. Miller, and D. Rind (2001), Northern Hemisphere winter climate response to greenhouse gas, ozone, and volcanic forcing, *J. Geophys. Res.*, *106*, 7193–7210.

Sigmond, M., and J. F. Scinocca (2010), The influence of basic state on the Northern Hemisphere circulation response to climate change, *J. Clim.*, *23*, 1434–1446, doi:10.1175/2009JCLI3167.1.

Sigmond, M., J. F. Scinocca, and P. J. Kushner (2008), Impact of the stratosphere on tropospheric climate change, *Geophys. Res. Lett.*, *35*, L12706, doi:10.1029/2008GL033573.

Son, S.-W., L. M. Polvani, D. W. Waugh, H. Akiyoshi, R. R. Garcia, D. E. Kinnison, S. Pawson, E. Rozanov, T. G. Shepherd, and K. Shibata (2008), The impact of stratospheric ozone recovery on the Southern Hemisphere westerly jet, *Science*, *320*, 1486, doi:10.1126/science.1155939.

Son, S. W., N. F. Tandon, L. M. Polvani, and D. W. Waugh (2009), Ozone hole and Southern Hemisphere climate change, *Geophys. Res. Lett.*, *36*, L15705, doi:10.1029/2009GL038671.

Stephenson, D. B., V. Pavan, M. Collins, M. M. Junge, and R. Quadrelli (2006), North Atlantic Oscillation response to transient greenhouse gas forcing and the impact on European winter climate: A CMIP2 multi-model assessment, *Clim. Dyn.*, *27*, 401–420.

Teyssèdre, H., et al. (2007), A new tropospheric and stratospheric Chemistry and Transport Model MOCAGE-Climat for multi-year studies: Evaluation of the present-day climatology and sensitivity to surface processes, *Atmos. Chem. Phys.*, *7*, 5815–5860.

Tian, W., and M. P. Chipperfield (2005), A new coupled chemistry-climate model for the stratosphere: The importance of coupling for future O_3-climate predictions, *Q. J. R. Meteorol. Soc.*, *131*, 281–303.

Uppala, S. M., et al. (2005), The ERA-40 re-analysis, *Q. J. R. Meteorol. Soc.*, *131*, 2961–3012, doi:10.1256/qj.04.176.

Volodin, E. M., and V. Y. Galin (1999), Interpretation of winter warming on Northern Hemisphere continents in 1977–94, *J. Clim.*, *12*, 2947–2955.

World Meteorological Organization (2007), Scientific assessment of ozone depletion: 2006, *Rep. 50*, 572 pp., Geneva, Switzerland.

H. Akiyoshi, T. Nakamura, and Y. Yamashita, National Institute of Environmental Studies, 16-2 Onogawa, Tsukuba, Ibaraki 305-8506, Japan.

S. Bekki, D. Cugnet, J. Jumelet, F. Lott, and M. Marchand, LATMOS-IPSL, Université Pierre et Marie Currie, 4, place Jussieu, F-75252 Paris Cedex 05, France.

P. Braesicke and J. A. Pyle, Centre for Atmospheric Science, Chemistry Department, Lensfield Rd., Cambridge University, Cambridge, CB2 1EW, UK.

N. Butchart and S. C. Hardiman, Hadley Centre, FitzRoy Rd., Exeter, EX1 3PB UK.

M. P. Chipperfield, S. S. Dhomse, and W. Tian, School of Earth and Environment, University of Leeds, Leeds, LS2 9JT, UK.

M. Deushi and K. Shibata, Meteorological Research Institute, Japan Meteorological Agency, 1-1 Nagamine, Tsukuba-City, Ibaraki 305-0052, Japan.

R. R. Garcia, A. Gettelman, D. E. Kinnison, and J.-F. Lamarque, National Center for Atmospheric Research, Box 3000, Boulder, CO 80307-3000, USA.

N. P. Gillett, D. Plummer, and J. F. Scinocca, Canadian Centre for Climate Modeling and Analysis, University of Victoria, PO Box 3065 STN CSC, Victoria, BC, V8W 3V6, Canada.

M. Michou, D. Olivié, D. Saint-Martin, H. Teyssèdre, and A. Voldoire, CNRM, Météo-France, 42 ave. Gustave Coriolis, F-31057 Toulouse Cedex, France.

O. Morgenstern and D. Smale, National Institute of Water and Atmospheric Research, Private Bag 50061, Omakau, 9352, New Zealand. (o.morgenstern@niwa.co.nz)

T. Peter, Institute for Atmospheric and Climate Science, ETH Zürich, Universitätstr. 16, CH-8092, Zürich, Switzerland.

E. Rozanov, Physical-Meteorological Observatory and World Radiation Center, Dorfstr. 33, CH-7260 Davos Dorf, Switzerland.

M. Sigmond, Department of Physics, University of Toronto, 60 St. George St., Toronto, ON, M5S 1A7, Canada.